Molecular Therapy
Nucleic Acids
Original Article

MicroRNA-494 Inhibits the LRG1 Expression to Induce Proliferation and Migration of VECs in Rats following Myocardial Infarction

Qiang Su,[1] Xiang-Wei Lv,[1] Yu-Han Sun,[2] Zi-Liang Ye,[2] Bing-Hui Kong,[2] and Zhen-Bai Qin[2]

[1]Department of Cardiology, Affiliated Hospital of Guilin Medical University, Guilin 541001, P.R. China; [2]Department of Cardiology, The First Affiliated Hospital of Guangxi Medical University, Nanning 530021, P.R. China

Myocardial infarction (MI) is a life-threatening cardiac event that results in extreme damage to the heart muscle. The Wnt signaling pathway has been implicated in the development of heart diseases. Hence, the current study aimed to investigate the role of microRNA (miRNA) in association with the Wnt signaling pathway to identify potential candidates for MI therapy. Differentially expressed miRNAs associated with MI occurrence were screened, and miR-494 was selected for subsequent experiments. Sprague-Dawley rats were included to establish a MI model via intraperitoneal injection of 0.1 mg/kg atropine sulfate and 40 mg/kg pentobarbital sodium. Then, the interaction between miR-494 and LRG1 was identified. The effect of miR-494 on expression of the Wnt signaling pathway-related genes, proliferation, migration, and invasion ability of fibroblasts and vascular endothelial cells (VECs) was subsequently evaluated through a series of gain- and loss-of-function experiments. The results revealed that miR-494 was poorly expressed and LRG1 was highly expressed in MI rats. miR-494 targets and downregulates LRG1, which resulted in the inactivation of the Wnt signaling pathway and promoted proliferation, migration, and invasion ability of fibroblasts and VECs. In conclusion, this study provided evidence suggesting that overexpressed miR-494 could potentially promote the proliferation, migration, and invasion of fibroblasts and VECs in MI through the inactivation of the Wnt signaling pathway by binding to LRG1.

INTRODUCTION

Myocardial infarction (MI) refers to myocardial necrosis-inflicted fibrous scar on living heart muscle.[1] Smoking has been identified as the underlying culprit of MI, along with gender, advancing age, and increasing deprivation, which have all been found to be responsible for a higher rate of MI.[2] In MI, hypofunctional fibroblasts have been reported to suppress the expression and diminish the migratory potential of several fibrosis-associated genes by inducing the impairment of myofibroblast trans-differentiation.[3] Encapsulated fibroblasts could stimulate the growth of vascular endothelial cells (VECs) in order to repair the damage caused to the ventricles following MI.[4] VECs serve as a regulator of blood pressure and can provide oxygen and nutrient supply to the heart during MI.[5] In the process of MI, acellular injectable biomaterial-based therapies have been employed to help regenerate and revive infarcted tissues.[6] Existing literature has highlighted the significant role of microRNAs (miRNAs or miRs) in the peripheral blood of patients with acute MI (AMI), which may also hold the key to potential MI treatment strategies.[7]

miR-494 plays an important role in the pathogenesis of cardiovascular disease through its involvement in specific signaling pathways.[8] Furthermore, miR-494 has been shown to facilitate the recovery of function owing to its ability to regulate the phosphate and tension homology deleted on chromosome 10/protein kinase B/mammalian target of rapamycin (PTEN/AKT/mTOR) signaling pathway in rats following spinal cord injury.[9] The bioinformatics website (http://www.microrna.org) provided data predicting that leucine-rich-alpha-2-glycoprotein 1 (LRG1) is a target gene of miR-494 and can be negatively regulated by miR-494. LRG1 has been identified to be positive in endothelial cells owing to its mitogenic activities, thus resulting in the improvement of angiogenesis.[10] Moreover, a previous study demonstrated that, in rats with middle cerebral artery occlusion, LRG1 could promote angiogenesis via the upregulation of the transforming growth factor-β (TGF-β) signaling pathway.[11] Another study also concluded that the migratory machinery of cells was associated with LRG1, because their activities were altered as observed in their performance within the non-canonical TGF-β signaling pathway.[12] Compelling evidence has identified the involvement of the Wnt signaling pathway in MI,[13,14] and that it was activated in MI as a potential therapeutic target.[14–16] The Wnt signaling pathway is known to serve as a stem cell pathway, which is critical for embryogenesis and the transcription of downstream members of the pathway.[17] Importantly, miR-494 has been reported to regulate the Wnt signaling pathway.[18] On the basis of aforementioned evidence, we proposed the hypothesis that miR-494 might potentially be

Received 19 November 2018; accepted 7 August 2019;
https://doi.org/10.1016/j.omtn.2019.08.007.

Correspondence: Qiang Su, Department of Cardiology, Affiliated Hospital of Guilin Medical University, No. 15, Lequn Road, Xiufeng District, Guilin 541001, Guangxi Zhuang Autonomous Region, P.R. China.
E-mail: suqiang1983@foxmail.com

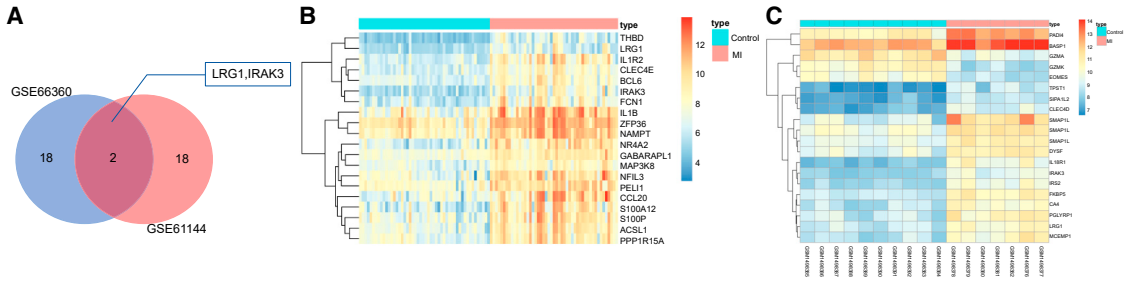

Figure 1. A Bioinformatic Prediction Method Was Adopted, Which Predicted miR-494 Targeting LRG1 via the Wnt Signaling Pathway as the Possible Molecular Mechanism for MI Therapy

(A) In the top 20 differentially expressed genes of GEO: GSE66360 and GSE61144 chips, there are two overlapped differentially expressed genes: IRAK3 and LRG1. (B and C) The differentially expressed gene expression heatmap of the 20 selected genes in GEO: GSE66360 and GSE61144, with the ordinate present for differentially expressed genes and the histogram in the upper right for color gradation in which each rectangle means a sample expression value (red, the highest sample expression; blue, the lowest sample expression).

involved in the development of MI via its interaction with LRG1, as well as the Wnt signaling pathway.

RESULTS

miR-494 Targeting LRG1 Affects MI via Regulating the WNT Signaling Pathway

Based on the two gene expression datasets related to MI, GEO: GSE66360 and GSE61144, along with the screening threshold of $p < 0.05$ and $|\text{LogFoldChange}| > 2$, differentially expressed genes related to MI were screened. Among the genes, the top 20 genes from each dataset were selected and then compared, after which a Venn diagram was plotted. As depicted in Figure 1A, there were two overlaps in the differentially expressed genes: IRAK3 and LRG1. The exact function of LRG1 in MI is yet to be fully understood. Therefore, we focused on the possible function of LRG1 in MI during our study. The heatmap of the top 20 differentially expressed genes retrieved in GEO: GSE66360 (Figure 1B) and GSE61144 (Figure 1C) datasets revealed that the expression of LRG1 was higher in patients with MI than that in normal individuals.

Next, miRDB and microRNA databases were applied to predict the potential miRNAs targeting LRG1, the results of which (Tables 1 and 2) revealed two overlaps: rno-miR-494-3p and rno-miR-873-5p, indicating that the two miRNAs were more likely to target LRG1. Based on the value of the Target Score or mirSVR score, rno-miR-494-3p had a higher Target Score but a relatively lower mirSVR score, highlighting the interaction between rno-494-3p and LRG1. Therefore, we focused on the role of miR-494 in LRG1. Numerous studies have revealed that the Wnt signaling pathway is activated in MI, which may provide a potential target for MI therapy.[14–16] Besides, miR-494 has been clarified to inhibit the Wnt signaling pathway.[18] On the basis of the aforementioned evidence, we subsequently concluded that miR-494 targets LRG1 via the Wnt signaling pathway.

Table 1. Bioinformatics Prediction of the Target Genes of miR-494 in miRDB in Patients with Myocardial Infarction

Target Rank	miRNA Name	Target Score
1	rno-miR-504	95
2	rno-miR-3562	84
3	rno-miR-494-3p	71
4	rno-miR-873-5p	58
5	rno-miR-3557-3p	58
6	rno-miR-24-3p	52

MI Rat Model Is Established Successfully

In order to examine whether the MI rat model had been successfully established, we analyzed pathological characteristics of the MI model rats and normal rats. The results revealed that in anterior descending coronary artery ligation, the myocardium pulsation below the ligation position was weakened, the myocardium became pale, the ST segment was elevated with increased T wave, and there was a significant elevation in lead II (Figure 2A). Ultrasonic cardiogram was performed at 24 and 48 h after MI in order to identify the inducing factors. It was observed that ejection fraction (EF) and fractional shortening (FS) were markedly decreased at 24 and 48 h, whereas the systolic left ventricular internal diameter was notably diminished at 48 h (Figures 2B and 2C). The aforementioned changes indicated that the MI rats exhibited all the expected MI symptoms, confirming that the model was established successfully.

Hemodynamic Detection Indicates Decreased Cardiac Functions of MI Model Rats

After observation of pathological characteristics, the cardiac functions of rats in the MI group and the sham group were measured in order to

Table 2. Bioinformatics Prediction of the Target Genes of miR-494 in MicroRNA in Patients with Myocardial Infarction

Target Rank	miRNA	mirSVR Score
1	rno-miR-494-3p	−0.9039
2	rno-miR-873-5p	−0.303
3	rno-miR-9a-5p	−0.2407

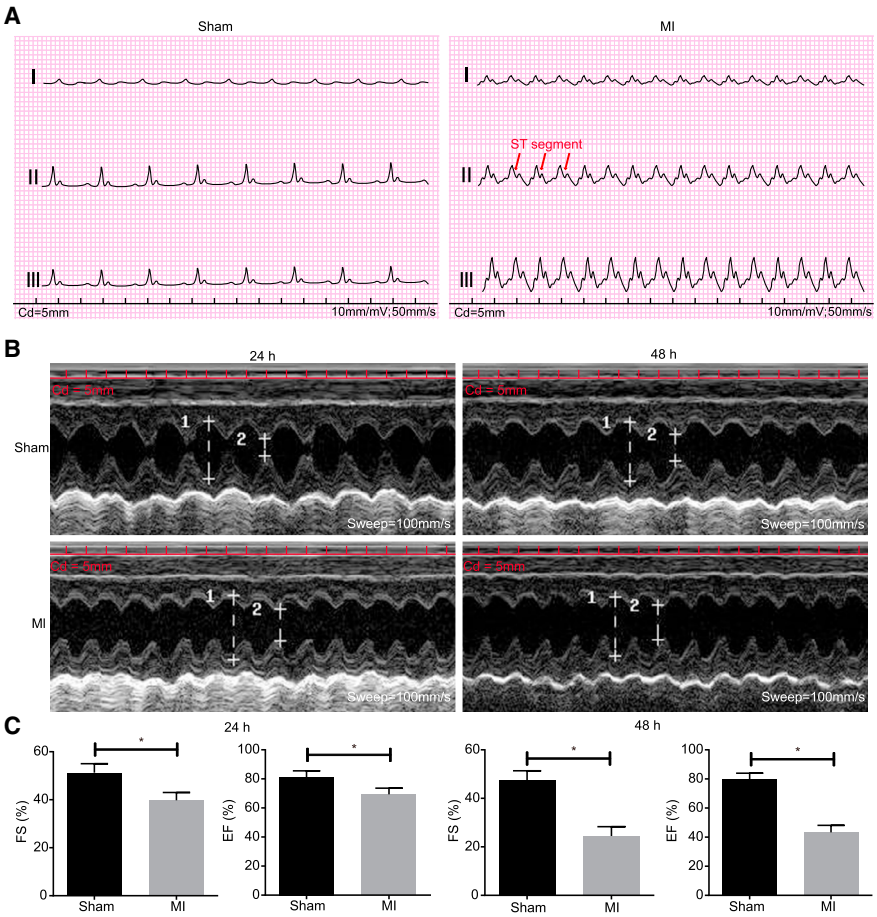

Figure 2. Electrocardiograms and Echocardiography of MI Rats and Normal Rats Show the Successfully Established MI Models (Sensitivity: 10 mm/mV; Paper Speed: 50 mm/s)

(A) Electrocardiogram of rats in the sham group indicated a rather smooth ST segment and T wave. (B) Representative M-mode images with end-diastole and end-systole indicated by arrows. (C) Measurements of FS and EF. Measurement data were expressed as mean ± SD. Statistical analysis was performed using an independent sample t test. *$p < 0.05$, **$p < 0.01$ versus the sham group. N = 20.

provide more biomarkers for MI occurrence. The detection results of left ventricular systolic pressure (LVSP), left ventricular end-diastolic pressure (LVEDP), maximal rate of increase of ventricular pressure (+dp/dtmax), and maximal rate fo decrease of ventricular pressure (−dp/dtmax) (Table 3) confirmed that, compared with rats in the sham group, the rats in the MI group had decreased LVSP, ± dp/dtmax, and increased LVEDP (all $p < 0.05$). The aforementioned results indicated that MI rats presented with weakened left ventricular systolic function, improved left ventricular diastolic function, and weakened cardiac systolic function and diastolic function.

MI Rats Present with Increased Infarct Size and Ventricular Mass Index

Further evaluation of myocardial function by 2,3,5-triphenyl tetrazolium chloride (TTC) staining (Figure 3) revealed that the healthy myocardium was stained red, whereas the ischemic tissue was stained white after TTC staining for 4–6 h. During left anterior descending artery (LAD) ligation, 100% of the myocardium was infracted (Figure 3A). Next, Evans blue staining was performed following MI to illustrate the persistence of infarcted tissue with the infarct size measured in accordance with the affected area (Figure 3B). The results revealed that the surviving myocardium was stained blue, whereas the affected area was red and the infarct size white. The infarct size was expressed as the percentage of affected area. We determined that the average infarct size was 32% during ligation operation (Figure 3C). Left ventricular mass index (LVMI) and right ventricular mass index (RVMI) of the rats in the MI group were much higher than those in the sham group ($p < 0.05$) (Figure 3D). These results suggested an increase in ventricular mass index in MI model rats.

MI Rats Exhibit Deteriorated Pathological Characteristics

The pathological characteristics of the myocardial tissues of the rats in each group were further assessed. Under a light microscope, the sham group had rounded myocardial cells aligned in a neat order, with

Table 3. Results of Hemodynamic Parameters (LVSP, LVEDP, and ± dp/dtmax) in Normal Rats and MI Rats

Group	N	LVSP (mm Hg)	LVEDP (mm Hg)	+dp/dtmax (mm Hg/ms)	−dp/dtmax (mm Hg/ms)
Sham	20	100.89 ± 10.34	7.44 ± 4.13	5.02 ± 0.39	−4.04 ± 0.31
Model	40	50.86 ± 7.92*	24.99 ± 8.05*	2.02 ± 0.34*	−2.61 ± 0.28*

Data are presented as mean ± SD. Statistical analysis was performed by Student's t test (two-sided). LVEDP, left ventricular end-diastolic pressure; LVSP, left ventricular systolic pressure; MI, myocardial infarction. *p < 0.05 versus the sham group.

clearly observed nuclei and complete cell membrane (Figure 4A). In the MI group, the cells displayed dissolved nuclei, karyotheca, and sarcolemma. The blood capillary of the MI rats was diminished and was replaced by a large amount of connective but disordered tissues. In addition, the MI rats also presented with myocyte necrosis, myoplasm agglomeration, and disorderly arranged cardiac muscle fibrous and strips with cytoplasm that occurred between the strong eosinophilic cross bands and deposited collagen fiber and more newborn blood capillary and inflammatory cells (Figure 4B). These observations indicated the deteriorated pathological function in MI model rats.

MI Rats Present with Increased Positive Expression of LRG1, α-SMA, and PCNA Proteins

The positive expression rate of LRG1, α−he positive expressioα-SMA), and proliferating cell nuclear antigen (PCNA) proteins was detected through the application of immunohistochemistry, the results (Figure 5) of which revealed that LRG1 and α-SMA were predominately located in the cytoplasm (Figure 5A), and PCNA was located in nuclei, in a myocardial cell inside the ischemic region, and in the fibroblasts surrounding the infarct region. Compared with the sham group, the positive expression rate of LRG1, α-SMA, and PCNA proteins was increased in the MI group ($p < 0.05$) (Figure 5B).

LRG1 Is a Target Gene of miR-494

A bioinformatics website and dual luciferase reporter gene assay were employed to verify the targeting relationship between miR-494 and LRG1. The online bioinformatics website (http://www.microrna.org) revealed there was a putative binding site between miR-494 and the 3′ UTR of LRG1 (Figure 6A). The results from the dual luciferase reporter gene assay (Figure 6B) indicated that there was a decrease in the luciferase activity in the LRG1-wild-type (WT) + miR-494 mimic group in comparison with that in the negative control (NC) group ($p < 0.05$), suggesting that the miR-494 mimic inhibited the luciferase activity, whereas no significant difference was detected between the LRG1 mutant (MUT) + miR-494 mimic group and the NC group ($p > 0.05$). The aforementioned results indicated that miR-494 targets and negatively regulates LRG1.

Lower Expression of miR-494, VEGF, and FGF, as well as Higher Expression of LRG1, Wnt-1, and β-Catenin in MI Rats

In order to detect the expression of miR-494 and LRG1 and the Wnt signaling pathway-related factors in MI rats, we conducted qRT-PCR assay (Figure 7A) and western blot analysis (Figures 7B and 7C). Compared with the sham group, miR-494 expression and mRNA and protein expression of vascular endothelial growth factor (VEGF) and fibroblast growth factor (FGF) in the MI group decreased, and mRNA and protein expression of LRG1, Wnt-1, and β-catenin exhibited notable increases ($p < 0.05$). Our results demonstrated that miR-494 was poorly expressed, LRG1 was highly expressed in rats with MI, and the Wnt signaling pathway was activated.

Overexpressed miR-494 Downregulates LRG1 Expression and Inhibits the Wnt Signaling Pathway

qRT-PCR (Figure 8A) and western blot analysis (Figures 8B and 8C) were performed in order to evaluate the expression of miR-494, VEGF, FGF, LRG1, Wnt-1, and β-catenin in myocardial fibroblasts and VECs after different transfections. The results illustrated that the mRNA and protein expression of LRG1, Wnt-1, and β-catenin was higher in the miR-494 inhibitor group when compared with the blank and NC groups, whereas the expression of miR-494, as well as the mRNA and protein expression of VEGF and FGF, was considerably lower in the miR-494 inhibitor group ($p < 0.05$). Meanwhile, in the miR-494 mimic and small interfering RNA (siRNA)-LRG1 groups, the mRNA and protein expression of LRG1, Wnt-1, and β-catenin was lower than that in the blank and NC groups, but that of VEGF and FGF was higher ($p < 0.05$). Compared with the blank and NC groups, greater miR-494 expression was identified in the miR-494 mimic group, whereas lower levels of miR-494 expression were detected in the miR-494 inhibitor + siRNA-LRG1 group ($p < 0.05$), with no significant difference detected in relation to the expression of LRG1, VEGF, FGF, LRG1, Wnt-1, and β-catenin in the siRNA-LRG1 group ($p > 0.05$). Furthermore, no significant difference was observed in relation to the expression of LRG1, miR-494, VEGF, FGF, LRG1, Wnt-1, and β-catenin between the blank group and the NC group ($p > 0.05$). The aforementioned results suggested that the overexpression of miR-494 could downregulate LRG1 and inhibit the Wnt signaling pathway.

Upregulated miR-494 Promotes the Proliferation of Fibroblasts and VECs by Silencing LRG1

In order to assess the cell proliferation ability following the transfection with different plasmids, we conducted 3-(4,5)-dimethylthiahiazo (-z-y1)-3,5-di-phenytetrazoliumromide (MTT) assay to calculate the relative cell proliferation rate by observing cell proliferation at 24, 48, and 72 h following transfection. The results (Figure 9) revealed no significant difference at 24 h ($p > 0.05$). At 48 and 72 h, the proliferation rate of fibroblasts and VECs had increased in the miR-494 mimic and siRNA-LRG1 groups, and the proliferation increased over the transfection time. Although the proliferation rate in the miR-494 inhibitor group slowed down and the discrepancy became clear gradually along the time ($p < 0.05$), there was no significant difference detected regarding the proliferation capacity in the miR-494 inhibitor + siRNA-LRG1 group in comparison with the blank and NC groups ($p > 0.05$). The above findings suggested that upregulated miR-494 could ease the proliferation of fibroblasts (Figure 9A, left) and VECs (Figure 9B, right) via inhibition of LRG1.

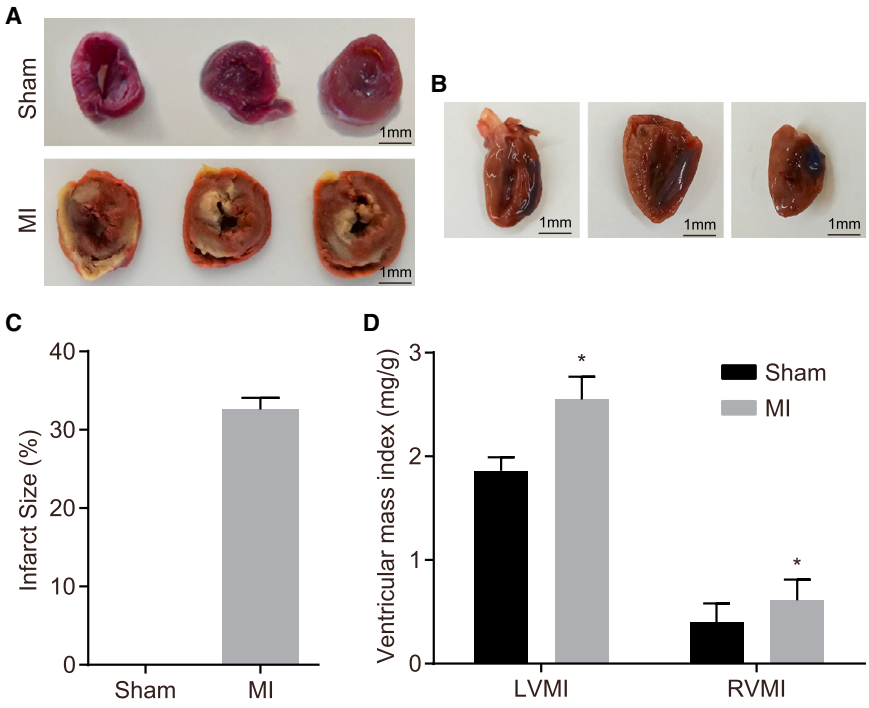

Figure 3. Infarct Size Increases and Cardiac Function Weakens in MI-Induced Rats

(A) Representative images of TTC-stained sham control and LAD-ligated hearts. Scale bars, 1 mm. (B) Representative images of Evans blue and TTC-stained LAD-ligated hearts after LAD ligation. Scale bars, 1 mm. (C) Histogram of infarct size in rats shows that infarct size is much larger in the MI group than in the sham group. (D) Ventricular mass index of rats in the sham and MI groups show that model rats have higher LVMI and RVMI. Measurement data were expressed as mean ± SD and analyzed using an independent sample t test. *$p < 0.05$ versus the sham group. N = 20.

Upregulated miR-494 Promotes Migration Ability of Fibroblasts and VECs by Silencing LRG1

The scratch test was performed to assess the migration ability of cells after transfection with different plasmids, the results of which are shown in Figures 10A and 10B. The results demonstrated that there was no significant difference in cell migration ability between the blank group and the NC group ($p > 0.05$). Compared with the blank and NC groups, migration ability of fibroblasts and VECs was enhanced in the miR-494 mimic and siRNA-LRG1 groups, whereas it was weakened in the miR-494 inhibitor group ($p < 0.05$), but no significant difference was found in the miR-494 inhibitor + siRNA-LRG1 group ($p > 0.05$). In addition, the results from the Transwell assay in relation to cell invasion ability were consistent with those obtained from the scratch test (Figures 10C and 10D). These findings provided evidence indicating that upregulated expression of miR-494 could accelerate migration and invasion ability of fibroblasts and VECs via silencing of LRG1.

DISCUSSION

LRG1 was found to be highly expressed in MI patients when analyzing the GEO: GSE66360 and GSE61144 microarray datasets for MI, and it was predicted to be regulated by miR-494 according to Target Score or mirSVR score. Previous studies have demonstrated that the activation of the Wnt signaling pathway in MI is a potential therapeutic target for MI.[15] Thus, we conducted a series of experiments in order to investigate the roles of miR-494, LRG1, and the Wnt signaling pathway in MI. Consequently, the results suggested that the overexpression of miR-494 can potentially promote the proliferation, migration, and invasion of fibroblasts and VECs in MI, which could be a potential mechanism for MI treatment.

MI and cardiovascular disease continue to place an enormous burden on society in high-income countries and developing countries.[2] A previous study revealed that LRG1 was involved in various human malignancies.[19] A study found that cardiac systolic function and diastolic function were weakened significantly in MI cases,[20] which were consistent with the findings of the current study. In addition, our study also demonstrated that MI rats had increased LVMI, RVMI, α-SMA, and PCNA. It has been reported that increased left ventricular mass and left ventricular hypertrophy are independent predictors of cardiovascular morbidity and mortality.[21] Distinct elevations in LVMI were reported in the MI group in a previous study, which was consistent with the observations of our study.[22] Furthermore, upregulated α-SMA and PCNA have been identified in the infarcted area of MI,[23,24] which was also in line with our study. *In vivo* experiments in this study revealed decreased levels of miR-494, VEGF, and FGF, but increased levels of LRG1, Wnt-1, and β-catenin in myocardial tissues of MI rats. The abnormal reduction of miR-494 has also been detected in leukemia.[25] VEGF has been shown to be stimulated in the process of myocardial ischemia and is thought to facilitate cardiovascular repair following AMI.[26] The overexpression of LRG1 has been detected in cancer issues, highlighting the potential involvement of LRG1 in MI treatment.[27] Zhao et al.[28] detected higher expression of Wnt-1 and β-catenin during their study in the myocardial tissues of MI rats.

In addition, *in vitro* experiments demonstrated that the overexpression of miR-494 or silencing of LRG1 resulted in the suppression of the expression of Wnt-1 and β-catenin, and increased expression of VEGF and FGF. Furthermore, the overexpression of miR-494 led to an increase in the proliferation, migration, and invasion of fibroblasts and VECs by inhibiting the Wnt signaling pathway. Collagen deposition, fibroblast proliferation, enhanced cardiomyocyte hypertrophy, and accelerated endothelial proliferation have all been identified as crucial elements involved in the recovery of MI.[29] The Wnt5A protein has been reported to be a consequence of the inhibition of human

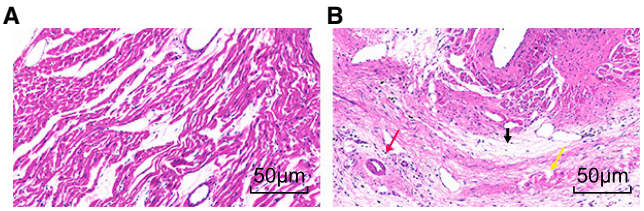

Figure 4. The TTC Staining Images Reflect Pathological Changes in the Myocardial Tissues in Rats that Underwent MI Inducement

(A) Myocardial tissues in the sham group display regular order and shape. (B) Myocardial tissues in the MI group show disorder arrangement, necrosis, collagen fibrous deposition, more new vessels, and inflammatory cells. The black arrow indicates collagen fibrous deposition, the red arrow indicates inflammatory cells, and the yellow arrow indicates necrosis. N = 20.

dental papilla cell proliferation and migration in MI.[30] Song et al.[18] presented evidence suggesting that the overexpression of miR-494 results in the inhibition of the Wnt signaling pathway. Furthermore, the tumor-suppressive role of miR-494 was also found in many cancers, including ovarian cancer and pancreatic cancer, through its ability in inhibiting cancer cell proliferation and invasion.[31,32] Likewise, the upregulation of miR-494 has been indicated to play a stimulatory role in hepatocellular carcinoma cell viability, migration, and invasion by suppressing PTEN expression and activating the PTEN/PI3K/AKT signaling pathway.[33] LRG1 has been suggested to be a new modulator of pathogenic angiogenesis and a novel oncogene-associated protein.[34] For example, the inhibition of tumor necrosis factor-α (TNF-α) could lead to the reduction in LRG1 expression.[35] TNF-α is widely considered to be an inducing factor triggering the local release of angiogenic substances, such as VEGF and basic FGF, which promoted the proliferation and migration of endothelial cells.[35] Additionally, the overexpression of LRG1 has been shown to diminish the migration and invasion of hepatocellular carcinoma cells.[36] Based on the target prediction program and the luciferase activity determination, we can conclude that LRG1 is a target gene of and is negatively regulated by miR-494.

In conclusion, the findings of our study demonstrate that overexpression of miR-494 could potentially accelerate the proliferation, migration, and invasion of fibroblasts and VECs in MI by inactivating the Wnt signaling pathway via inhibition of LRG1 (Figure S1). However, further experiments are still required to further elucidate the specific mechanism by which miR-494 influences MI with the involvement of LRG1 and the Wnt signaling pathway.

MATERIALS AND METHODS

Ethics Statement

All animal experiments in the present study were carried out in strict accordance to the recommendations in the Guide for the Care and Use of Laboratory Animals and in line with the requirements of the Ethics Committee in Affiliated Hospital of Guilin Medical University. All animals in this study were treated with any possible means to relieve their pain.

Microarray-Based Gene Expression Profiling

The gene expression datasets regarding MI (GEO: GSE66360 and GSE61144) were obtained from the GEO (https://www.ncbi.nlm.nih.gov/geo/). GEO: GSE66360 contained the expression data of the circulating endothelial cells (CECs) collected from 49 MI patients and 50 normal individuals, with the annotation platform GPL570-[HG-U133_Plus_2] Affymetrix Human Genome U133 Plus 2.0 Array. GEO: GSE61144 contained the expression data of the blood samples from 7 MI patients and 10 normal individuals, using annotation platform GPL6106-Sentrix Human-6 v2 Expression Bead Chip. The Affy package of R language was applied for background correction and normalization pre-processing.[37] The linear model-empirical Bayes statistical method combined with traditional t test in the Limma package of R language was used to carry out a nonspecific filtration process for screening the differentially expressed mRNAs.[38] The screening threshold for the differentially expressed genes was $p < 0.05$ and $|\text{LogFoldChange}| > 2$. Next, a heatmap of the differentially expressed genes was plotted. Finally, the online analysis tool "Calculate and draw custom Venn diagrams" (http://bioinformatics.psb.ugent.be/webtools/Venn/) was utilized to compare the differentially expressed genes of the two datasets with the overlapped genes identified and recorded. miRDB (http://www.mirdb.org/) and microRNA (http://www.microrna.org/microrna/microrna/getGeneForm.do) were the two prediction tools used to analyze the relationship between miRNAs and mRNAs, which can be used to predict the miRNAs capable of regulating the relevant differentially expressed genes.

Establishment of MI Rat Models

Eighty-four specific pathogen-free Sprague-Dawley rats (42 males and 42 females, weight: 210–250 g) provided by the Laboratory Animal Center of Guilin Medical University Fuwai Hospital of Cardiovascular Disease (Beijing, China) were raised under conventional conditions for a week and subsequently anaesthetized through the intraperitoneal injection with 0.1 mg/kg atropine sulfate (091203; Taiji Group Southwest Pharmaceutical, Chongqing, China) and 40 mg/kg pentobarbital sodium (Shanghai Sino Pharm, Shanghai, China). Once the righting response was observed to have disappeared, the rats were fixed in a supine position with the skins of the neck cut open and the skin of the chest removed, sterilized three times with the iodine complex disinfection solution, and draped with well sheets. The neck skin was cut open under sterile condition in order to isolate the neck muscles by blunt dissection, in order to expose the trachea. An incision of 2 mm was made transversely on the trachea between two and three cartilaginous rings of the thyroid. Next, tracheal intubation was performed to maintain respiration by connecting a mini animal respirator (Model: ALS-V8S; respiratory rate: 70 breaths/min; respiratory ratio: 1:1; tidal volume: 10–12 mL; Shanghai Alcott Biotechnology, Shanghai, China) to cut open the trachea. Next, the skin on the left side of the chest was cut open; the muscles were isolated by blunt dissection; and the third and fourth ribs were separated longitudinally to tear open the pericardium with ophthalmic forceps until the full exposure of the heart of the rat was obtained. The surface of the myocardium below the LAD coronary artery was penetrated by

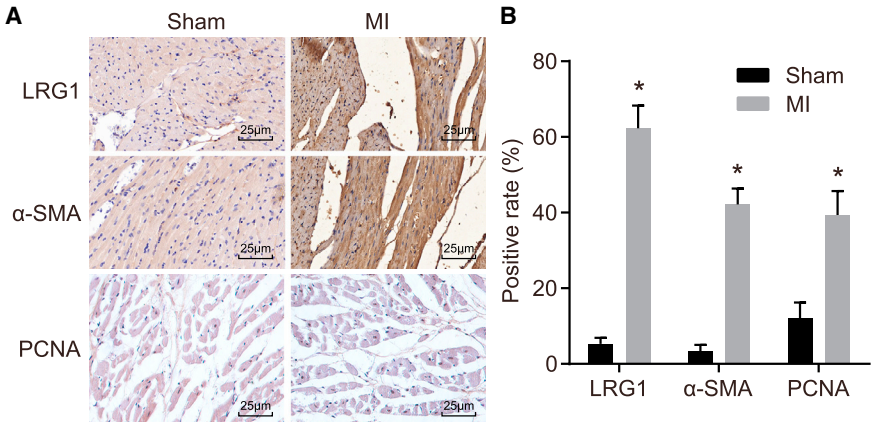

Figure 5. Pathological Changes and Necrosis Are Observed, and Positive Expression of LRG1, α-SMA, and PCNA Is Higher in Rats that Underwent MI Inducement

(A) Staining images of LRG1, α-SMA, and PCNA in rats from the sham and MI groups. (B) Positive expression of LRG1, α-SMA, and PCNA in rats is higher in the MI group than in the sham group. Data followed normal distribution, were expressed as mean ± SD, and were analyzed by an independent sample t test. *$p < 0.05$ versus the sham group. N = 20.

No. 5-0 sutures at 1 mm of the left margin of the pulmonary artery and the lower right margin of the left atrial appendage. When the color of the myocardium below the ligature area became pale, along with gradually weakened pulsation and obviously elevated ST segment, the MI rat model was established successfully. Afterward, the chest of the rats was then closed under negative pressure, with the chest wall and skin sutured layer by layer followed by removal of the respirator. The skin of the neck was sutured and sterilized with the iodine complex solution. Within 3 days after the operation, the rats were administrated with intraperitoneal injection of penicillin (2×10^4 U/day) to avoid infection. For rats in the sham group, the sutures were made without ligation of coronary arteries (n = 20), whereas the other manipulations were the same as the MI group. Forty-two out of 64 rats with ligation of the anterior descending coronary artery survived, with 40 of those that survived randomly selected and regarded as the MI group.

Cardiac Function Evaluation

The rats were anesthetized in a sealed chamber containing 5% isoflurane until cessation of movement (about 30 s). The pup was secured in the supine position on a heated dock at 37°C with its nose in a cone for delivery of 0.5%–1% isoflurane to maintain anesthesia. Prewarmed echo gel was placed on the left thoracic area. A parasternal long-axis view of the left ventricle was obtained with the images below the level of the suture in the left ventricle acquired. After the position had been identified, the ultrasound probe (40 MHz) was rotated to 90° in order to obtain a parasternal short-axis view with M-mode echocardiographic images recorded. The end-diastolic and end-systolic left ventricular internal diameters were measured from the short-axis M-mode images, after which the EF and FS were calculated.

Detection of the Hemodynamic Index

The hemodynamic study was conducted in the MI group and the sham group. The rats were anesthetized through intraperitoneal injection of 0.1 mg/kg atropine sulfate solution and 40 mg/kg pentobarbital sodium. When the rats showed no righting response, they were fixed in a supine position. One end of the arterial pressure tube was connected to hypodermic needles (1.5G), and the other end with a four-channel physiological recorder (AD Instrument; Model: Powerlab/4SPML750). When the hypodermic needle was pushed slowly from the apex to the left ventricle of the heart, the oscilloscope was observed and the pushing was terminated once the needle had been fully pushed into the left ventricle. After the needle had been confirmed to have remained in the left ventricle for 3 s, LVSP, LVEDP, dp/dtmax, and −dp/dtmax of the left ventricle were recorded.

Measurement of Ventricular Mass Index and Infarct Size in Rats

The infarct size of the MI rats was measured following TTC staining. After hemodynamic index measurement, the rats were euthanized through the injection of 10% KCl (3 mL). Next, the rat chest was opened in order to obtain the heart, after which the atria and the great vessels were separated, followed by separation of the left and right ventricle (including ventricular septum). The heart specimens were washed with normal saline and then frozen at −20°C for 10 min. After the samples were frozen, serial sections of 2–3 mm were made along with the vertical direction of the long axis of the heart from the apex to the bottom of the heart until it reached a parallel level of the ligation line. The sections were later stained in TTC dye liquor (DK0004; Shanghai Jing Ke Chemical Technology, Shanghai, China) at 37°C for 20 min devoid of light exposure and fixed for 15 min using 4% formaldehyde solution. The infarct size in red or pale color was separated using a scissor and subsequently weighed. Meanwhile, the left ventricle and right ventricle were also separately weighed, after which the body mass was recorded. The LVMI and RVMI were calculated as: left (right) ventricle weight/body mass, and the infarct size as muscle weight of MI in the left ventricle/left ventricular muscle mass (LVMM) under the ligation line × 100%.

H&E Staining

Myocardial tissue sections were prepared in order to analyze the pathological changes through H&E staining. The apex part of the sections (4 μm) was dehydrated at 55°C–65°C for 1–2 h; dewaxed with xylene I for 10 min and xylene II and III for 5 min; and later dewaxed and hydrated by ethanol-water washing for 2 min, followed by hematoxylin staining for 5 min and washing under running water. After staining, the sections were differentiated using 0.25% hydrochloric

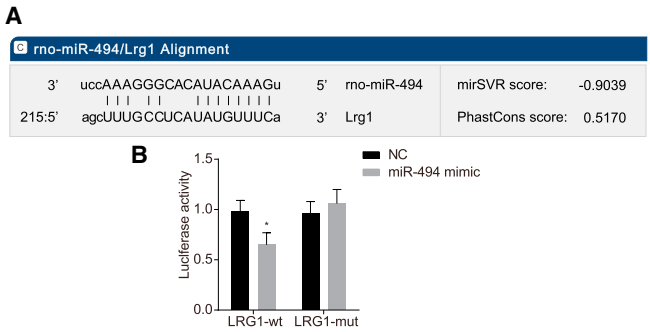

Figure 6. Dual Luciferase Reporter Gene Assay and Bioinformatics Prediction Indicate that LRG1 Is Negatively Regulated by miR-494

(A) The putative miR-494 binding site in the 3′ UTR of LRG1. (B) Dual luciferase reporter gene assay result demonstrates that luciferase activity is higher in the miR-494 mimic group than in the NC group. Data followed normal distribution, were expressed as mean ± SD, and were analyzed by an independent sample t test. *$p < 0.05$ versus the NC group. The experiment was repeated three times.

acid-ethanol for 3–5 s, further stained by blue liquor for a while and with eosin for 20 s. After dehydration with ethanol for 10 min and dewaxing by xylene I and II separately for 5 min, the sections were sealed by neutral balsam. Pathological changes of myocardial tissues were observed under an optical microscope (DMM-300D; Shanghai Caikon Optical Instrument, Shanghai, China).

Immunohistochemistry

The myocardial tissues were conventionally fixed, paraffin embedded, and cut into sections, followed by incubation in 3% H_2O_2 for 10–15 min at room temperature to inactivate endogenous peroxidase. Immunohistochemical staining was performed on the myocardial tissues in accordance with the instructions provided by the PV-6001 Power Vision TM Two-Step kit (Beijing Zhongshan Golden Bridge Biotechnology, Beijing, China). In brief, the tissue sections were incubated with the following rabbit polyclonal antibodies purchased from Abcam (Cambridge, MA, USA): LRG1 (ab181882; 1:500), α-SMA (ab28379; 1:100), and PCNA (ab18197; 1:1,000) at 37°C for 30 min and overnight at 4°C. After conventional washing, the sections were then incubated with secondary antibody goat anti-rabbit immunoglobulin G (IgG) and V_HH fragments (single-domain antibody; ab191866; 1:1,000; Abcam, Cambridge, MA, USA) at 37°C for 30 min and subsequently colored with diaminobenzidine. PBS was used as the primary antibody and regarded as the NC. Six visual fields under a light microscope (×200) were randomly selected from each section and analyzed using Image-Pro Plus 5.0 software. The protein expression of LRG1, α-SMA, and PCNA was subsequently evaluated by positive staining area/total area. When LRG1 presented with yellow granules, α-SMA presented with yellow fine particles, and PCNA presented with yellow circle particles, they were considered to be positive protein expression.

Dual Luciferase Reporter Gene Assay

The online bioinformatics website (http://www.microrna.org) provided predictor data indicating that LRG1 was a direct target gene of miR-494. The 3′ UTR of LRG1 was amplified by PCR and cloned into Psicheck-2 vector to construct the WT and MUT of LRG1 for evaluation by dual luciferase reporter gene assay. Target gene fragments were inserted into pMIR-reporter at the endonuclease sites of SpeI and Hind III, and the MUT site of the target sequence was designed based on LRG1-MUT, which was later digested by restriction enzyme and inserted into the pMIR-reporter genes by ligase. WT and MUT dual luciferase reporter genes with correctly identified sequences were co-cultured with miR-494 into HEK293T cells and divided into the LRG1-WT + NC group, LRG1-WT + miR-494 mimic group, LRG1-MUT + NC group, and LRG1-MUT + miR-494 mimic group. The luciferase activity of cells in each group was determined after 48-h transfection. The mean value was obtained and recorded following three independent experiments.

RNA Isolation and Quantification

Myocardial tissues of 100 mg were extracted and ground into fine powder in liquid nitrogen. The ground tissue samples were mixed with 1,000 μL TRIzol homogenization (Invitrogen, Carlsbad, CA, USA) followed by centrifugation for supernatant collection. Following chloroform extraction, isopropanol precipitation, ethanol washing, dissolution in 0.01% diethyl pyrocarbonate, and RNA precipitation, total RNA was extracted and reserved at −70°C prior to use. The concentration and purity of the extracted RNA were evaluated using a violet spectrophotometer (Perkin Elmer, Waltham, MA, USA). After the concentration and purity of the RNA were determined, a total of 2 μg RNA was reversely transcribed into cDNA.

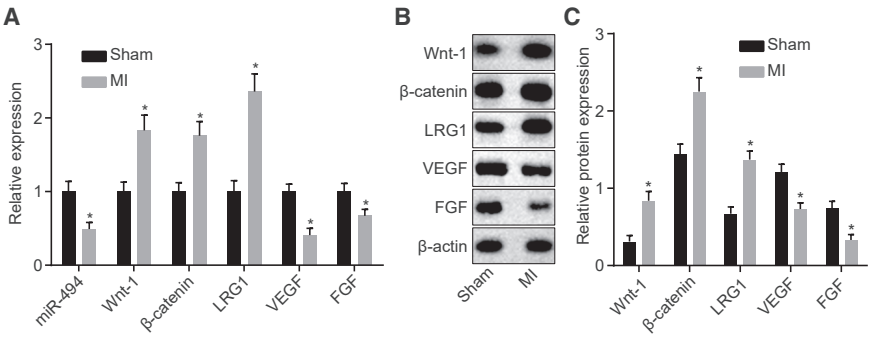

Figure 7. The Expression of Wnt-1, β-Catenin, and LRG1 Increases and Expression of miR-494, VEGF, and FGF Decreases in the Cells with MI Induction

(A) qRT-PCR for assessing the expression of Wnt-1, β-catenin, LRG1, miR-494, VEGF, and FGF in the sham and MI groups normalized to the sham group. (B and C) Western blot analysis for analyzing the expression of Wnt-1, β-catenin, LRG1, VEGF, and FGF in the sham and MI groups normalized to β-actin. Data were presented as means ± SD. Statistical analysis was performed by Student's t test. *$p < 0.05$ versus the sham group. The experiment was repeated three times.

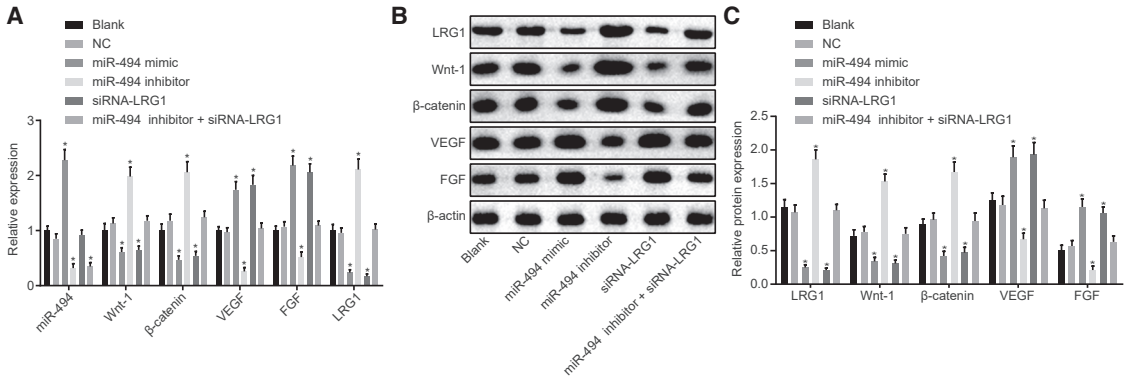

Figure 8. The RT-qPCR and Western Blot Analysis Reveal that Overexpression of miR-494 Suppresses LRG1 and Inhibits the Wnt Signaling Pathway

(A) qRT-PCR for assessing the expression of Wnt-1, β-catenin, LRG1, miR-494, VEGF, and FGF in cells after transfection of different mimic, inhibitor, or siRNA normalized to the blank group. (B and C) Western blot analysis for analyzing the expression of Wnt-1, β-catenin, LRG1, VEGF, and FGF in cells after transfection of different mimic, inhibitor, or siRNA normalized to β-actin. Data followed normal distribution, were expressed as means ± SD, and were analyzed by one-way ANOVA, followed by Tukey's post hoc test. The experiment was repeated three times. *$p < 0.05$ versus the blank and NC groups.

The PCR primers (Table 4) were designed using the Primer Express 2.0 software with the primers provided by Nanjing Genscript (Nanjing, Jiangsu, China). β-Actin was regarded as the internal control. The relative expression of target genes was calculated using the $2^{-\Delta Ct}$ method. The aforementioned method was also suitable for cell experiment.

Western Blot Analysis

The myocardial tissues were ground into fine powder in liquid nitrogen and subsequently extracted using cell lysate of radio immunoprecipitation assay and phenylmethyl sulfonylfluoride. The extracted proteins were quantified using the modified Bradford method, followed by protein purification and separation using PAGE. The separated proteins were transferred onto a nitrocellulose membrane. The membrane was then blocked with 5% skimmed milk powder, washed by Tris-buffered saline-Tween-20 (TBST) (pH 7.4), and incubated overnight at 4°C with the following rabbit polyclonal antibodies purchased from Abcam (Cambridge, MA, USA): LRG1 (ab181882, 1:500), β-actin (ab8227, 1:1,000), β-catenin (ab16051, 1:1,000), Wnt-1 (ab15251, 1:200), VEGF (ab11939, 1:1,000), and FGF (ab16828, 1:1,000). Subsequently, the membrane was reacted with secondary antibodies of goat anti-rabbit IgG and V_HH fragments (single-domain antibody) (ab191866, 1:1,000; Abcam, Cambridge, MA, USA) for 1 h at room temperature, followed by development using enhanced chemiluminescence and visualization using an X-ray machine with corresponding images acquired by a gel imaging instrument (GIS 2012; Tanon Science & Technology, Shanghai, China). β-Catenin was employed as an internal reference. The relative protein expression was calculated based on the ratio of gray value of target protein to that of internal control, the results of which were analyzed by SPSS 21.0 software (IBM, Armonk, NY, USA). The analysis of categorical data was conducted by chi-square test. The method was also applicable to cell experiments.

Cell Treatment

Myocardial tissues of 3 mm were separated and treated with 3 mL enzyme digestion solution at 37°C for 15 min and then naturally precipitated for 1 min followed by removal of the supernatant. After that, the samples were centrifuged for further primary cell culture. When the cells reached 80%–90% confluence, the fibroblasts and VECs in the logarithmic growth phase were seeded into six-well plates, respectively. When the cells had reached 30%–50% confluence, they were transfected in strict accordance with the instructions of Lipofectamine 2000 (Invitrogen, Carlsbad, CA,

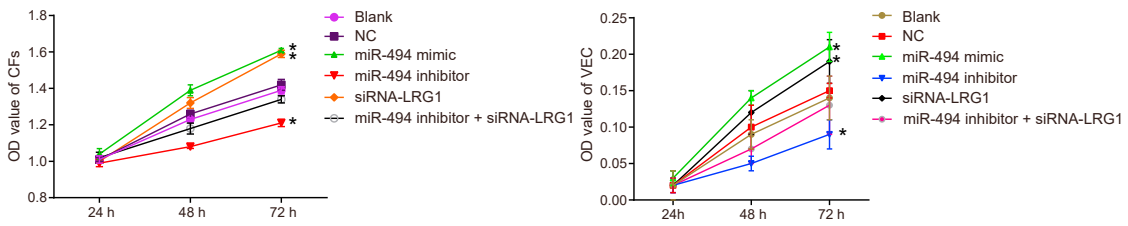

Figure 9. The MTT Assay Shows that Upregulation of miR-494 or Silencing LRG1 Promotes the Proliferation Ability of Fibroblasts and VECs

(A) Proliferation ability of fibroblasts after transfection with different plasmids for 24, 48, and 72 h. (B) Proliferation ability of VECs after transfection with different plasmids for 24, 48, and 72 h. Data following normal distribution were expressed as means ± SD and analyzed by repeated-measures ANOVA. The experiment was repeated three times. *$p < 0.05$ versus the blank and NC groups.

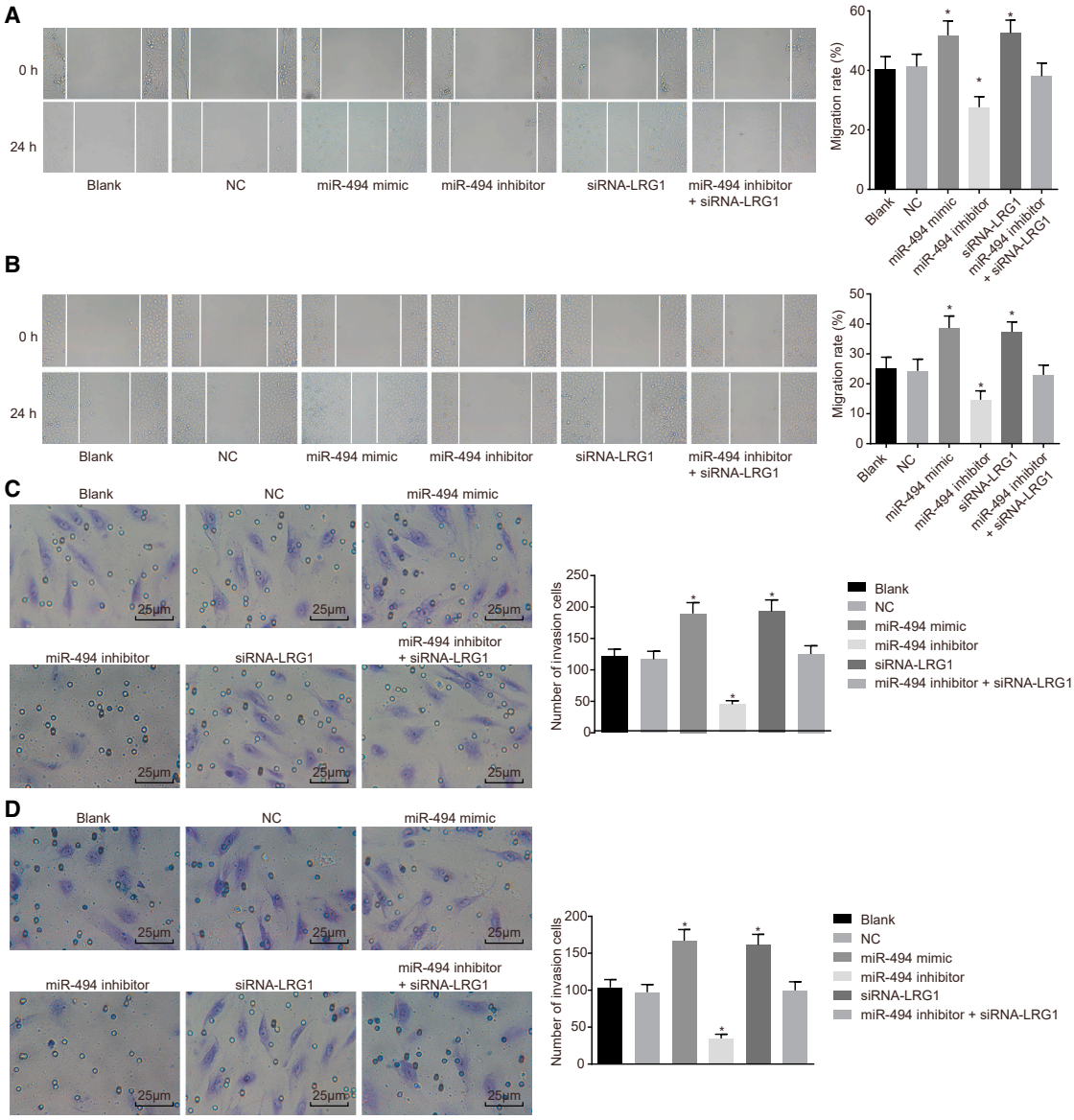

Figure 10. Scratch Test Shows that Upregulation of miR-494 or Silencing LRG1 Promotes Migration and Invasion Ability of Fibroblasts and VECs

(A) Migration ability of fibroblasts based on the scratch widths in different transfection groups. (B) Migration ability of VECs in different transfection groups. (C) Invasion ability of fibroblasts detected by Transwell assay in different transfection groups. (D) Invasion ability of VECs detected by Transwell assay in different transfection groups. Data following normal distribution were expressed as means ± SD and analyzed by one-way ANOVA, followed by Tukey's post hoc test. *$p < 0.05$ versus the blank and NC groups. The experiment was repeated three times.

USA). The serum-free Opti-MEM of 250 μL (GIBCO, Grand Island, NY, USA) was used to dilute 100 pmol of miR-494 mimic, miR-494 inhibitor, siRNA-LRG1, miR-494 inhibitor + siRNA-LRG1, and NC, and mixed and incubated at room temperature for 5 min. Next, 5 μL Lipofectamine 2000 was diluted by 250 μL serum-free Opti-MEM medium, followed by incubation at room temperature for 5 min. The aforementioned two were then mixed and incubated for an additional 20 min at room temperature prior to being added to the cell culture wells for incubation with 5% CO_2 at 37°C for 6–8 h. After the culture medium was replaced by complete medium, the samples were cultured for another 24–48 h. The final cultured cells were assigned into six groups, namely, the blank group (cells transfected with empty vector), NC group (cells transfected with NC vector), miR-494 mimic group (cells transfected with miR-494 mimic), miR-494 inhibitor group (cells transfected with miR-494 inhibitor), siRNA-LRG1 group (cells transfected with siRNA-LRG1), and miR-494 inhibitor + siRNA-LRG1 group (cells co-transfected with miR-494 inhibitor and siRNA-LRG1).

Table 4. Primer Sequences of Target Genes by qRT-PCR

Genes	Forward Primer (5′–3′)	Reverse Primer (5′–3′)
miR-494	TGGTGATGGGATTTGAAACAT ACACGGGAAAC	AGATAGACGGTGTC GCTGTTGAAGTCAG
LRG1	GACAGCGACCAAAAAGCCCAG	GCAGGTGGTCAGG TTGAA
β-Ccatenin	GCTGACCAAACTGCTA AATGAGGA	TGATAGGGTCCCAG CGGTACAA
Wnt-1	GCCAACAGTAGTGGCCGATG	CTGGGCTCTAGCA CCAGCTGTA
VEGF	CGGTGTGGTCTTTCGTCCTTC	GGTTTGTCGTGTTTC TGGAAGTG
FGF	AAAGGCAATCTTCGGGAGTA	TGATAGGCACAGG ACACCAG
β-Actin	GGAGATTACTGCCCTGG CTCCTA	GACTCATCGTACT CCTGCTTGCTG

FGF, fibroblast growth factor; LRG1, leucine-rich-alpha-2-glycoprotein 1; miR, microRNA; VEGF, vascular endothelial growth factor.

MTT Assay

Fibroblasts and VECs in the logarithmic growth phase were treated with trypsin and re-suspended with the complete medium into a cell suspension, with the cell number counted using a blood cell counting chamber. The cells were then seeded in a 96-well plate at a density of 5.0×10^3 cells/well. Following adherence for 12 h, the cells were cultured in serum-free Opti-MEM with five parallel wells in each group, and 200 μL of cell suspension was added into each group. Cell proliferation in each group was examined continuously for 2 days, with the same number of cells added into each well. Following transfection for 6 h, the culture medium containing transfection reagent was replaced with a normal medium containing serum, and the plate was incubated at 37°C with 5% CO_2 for 2 days under conditions void of light. Then, 20 μL 0.5% MTT storage solution (5 mg/mL) was added into each well for a further 4-h incubation. Next, the culture medium in the 96-well plate was removed with a 5-mL syringe, and 150 μL DMSO was added to each well, after which incubation was performed while vibrating for 10 min at a low speed in order to fully dissolve the blue crystal. The absolute optical density (OD) value of each well was measured with a multi-function microplate reader at an excitation wavelength of 490 nm. The experiment was conducted in triplicate to obtain average value.

Scratch Test

After 48-h transfection, residual fluid was discarded from the culture plate and cells were centrifuged to remove the culture medium after cell detachment. After that, the cells were re-suspended with serum-free medium containing BSA. The cell density was adjusted to 1.0×10^6 cells/mL, after which 100 μL of cell suspension was extracted. The cells in the logarithmic growth phase were seeded into a six-well plate and cultured with 5% CO_2 at 37°C. When the cells reached 80% confluence, a thin wound was created along the center axis of each well with a 20-μL sterile pipette tip. The suspended cells were washed away with three sterile PBS (pH 7.4) washes. The cells in the six-well plate were cultured in 2 mL complete medium at 37°C. The scratch widths when the scratch was created (0 h) and after 24-h incubation were observed with the rate of cell migration calculated by Image-Pro Plus 6.0. The experiment was performed three times independently, and triplicate wells were set in each experiment, followed by statistical analysis.

Transwell Assay

The Matrigel-coated Transwell chambers were pre-heated to 37°C. The transfected cells were detached, washed twice with serum-free medium, and re-suspended in serum-free medium, followed by cell counting with the cell density adjusted to 1×10^5 cells/mL. Next, 600 μL RPMI 1640 medium containing 20% fetal bovine serum was added to the basolateral chambers, whereas 200 mL of cell suspension was added to the apical chambers for 48-h culture at 37°C. The Transwell chambers were then taken out, and the cells on the apical chambers were removed. Following a PBS wash, the cells were fixed in 4% paraformaldehyde for 10 min, stained with crystal violet, and observed under an optical microscope with images obtained. Five high-power fields of view were randomly selected. Triplicate wells were set for each group. The experiment was conducted in triplicate to obtain the mean value.

Statistical Analysis

All experimental data were analyzed using SPSS 21.0 (IBM, Armonk, NY, USA). All data followed normal distribution and homogeneity of variance. Measurement data were expressed as mean ± SD. Comparisons between two groups were analyzed by t test, and comparisons among multiple groups were assessed by one-way ANOVA, followed by Tukey's post hoc test. $p < 0.05$ was considered of statistically significant difference.

SUPPLEMENTAL INFORMATION

Supplemental Information can be found online at https://doi.org/10.1016/j.omtn.2019.08.007.

AUTHOR CONTRIBUTIONS

Q.S., X.-W.L., and Y.-H.S. designed the study. Q.S., Z.-L.Y., and B.-H.K. collated the data, carried out data analyses, and produced the initial draft of the manuscript. X.-W.L. and Z.-B.Q. contributed to drafting the manuscript. All authors have read and approved the final submitted manuscript.

CONFLICTS OF INTEREST

The authors declare no competing interests.

ACKNOWLEDGMENTS

We acknowledge and appreciate our colleagues for their valuable efforts and comments on this paper. This work was supported by Natural Science Foundation of Guangxi Zhuang Autonomous Region (grant 2017GXNSFAA198069).

REFERENCES

1. Makkar, R.R., Smith, R.R., Cheng, K., Malliaras, K., Thomson, L.E., Berman, D., Czer, L.S., Marbán, L., Mendizabal, A., Johnston, P.V., et al. (2012). Intracoronary cardiosphere-derived cells for heart regeneration after myocardial infarction (CADUCEUS): a prospective, randomised phase 1 trial. Lancet *379*, 895–904.
2. Feary, J.R., Rodrigues, L.C., Smith, C.J., Hubbard, R.B., and Gibson, J.E. (2010). Prevalence of major comorbidities in subjects with COPD and incidence of myocardial infarction and stroke: a comprehensive analysis using data from primary care. Thorax *65*, 956–962.
3. Dobaczewski, M., Bujak, M., Li, N., Gonzalez-Quesada, C., Mendoza, L.H., Wang, X.F., and Frangogiannis, N.G. (2010). Smad3 signaling critically regulates fibroblast phenotype and function in healing myocardial infarction. Circ. Res. *107*, 418–428.
4. Hunt, N.C., Shelton, R.M., Henderson, D.J., and Grover, L.M. (2013). Calcium-alginate hydrogel-encapsulated fibroblasts provide sustained release of vascular endothelial growth factor. Tissue Eng. Part A *19*, 905–914.
5. Bharadwaj, A.S., Appukuttan, B., Wilmarth, P.A., Pan, Y., Stempel, A.J., Chipps, T.J., Benedetti, E.E., Zamora, D.O., Choi, D., David, L.L., and Smith, J.R. (2013). Role of the retinal vascular endothelial cell in ocular disease. Prog. Retin. Eye Res. *32*, 102–180.
6. Hernandez, M.J., and Christman, K.L. (2017). Designing Acellular Injectable Biomaterial Therapeutics for Treating Myocardial Infarction and Peripheral Artery Disease. JACC Basic Transl. Sci. *2*, 212–226.
7. Guo, M.L., Guo, L.L., and Weng, Y.Q. (2017). Implication of peripheral blood miRNA-124 in predicting acute myocardial infarction. Eur. Rev. Med. Pharmacol. Sci. *21*, 1054–1059.
8. Wu, A., Lou, L., Zhai, J., Zhang, D., Chai, L., Nie, B., Zhu, H., Gao, Y., Shang, H., and Zhao, M. (2017). miRNA Expression Profile and Effect of Wenxin Granule in Rats with Ligation-Induced Myocardial Infarction. Int. J. Genomics *2017*, 2175871.
9. Zhu, H., Xie, R., Liu, X., Shou, J., Gu, W., Gu, S., and Che, X. (2017). MicroRNA-494 improves functional recovery and inhibits apoptosis by modulating PTEN/AKT/mTOR pathway in rats after spinal cord injury. Biomed. Pharmacother. *92*, 879–887.
10. Wang, X., Abraham, S., McKenzie, J.A.G., Jeffs, N., Swire, M., Tripathi, V.B., Luhmann, U.F.O., Lange, C.A.K., Zhai, Z., Arthur, H.M., et al. (2013). LRG1 promotes angiogenesis by modulating endothelial TGF-β signalling. Nature *499*, 306–311.
11. Meng, H., Song, Y., Zhu, J., Liu, Q., Lu, P., Ye, N., Zhang, Z., Pang, Y., Qi, J., and Wu, H. (2016). LRG1 promotes angiogenesis through upregulating the TGF-β1 pathway in ischemic rat brain. Mol. Med. Rep. *14*, 5535–5543.
12. Lynch, J., Fay, J., Meehan, M., Bryan, K., Watters, K.M., Murphy, D.M., and Stallings, R.L. (2012). MiRNA-335 suppresses neuroblastoma cell invasiveness by direct targeting of multiple genes from the non-canonical TGF-β signalling pathway. Carcinogenesis *33*, 976–985.
13. Tao, J., Wang, Y.T., Abudoukelimu, M., Yang, Y.N., Li, X.M., Xie, X., Chen, B.D., Liu, F., He, C.H., Li, H.Y., and Ma, Y.T. (2016). Association of genetic variations in the Wnt signaling pathway genes with myocardial infarction susceptibility in Chinese Han population. Oncotarget *7*, 52740–52750.
14. Hermans, K.C., Daskalopoulos, E.P., and Blankesteijn, W.M. (2012). Interventions in Wnt signaling as a novel therapeutic approach to improve myocardial infarct healing. Fibrogenesis Tissue Repair *5*, 16.
15. Bastakoty, D., Saraswati, S., Joshi, P., Atkinson, J., Feoktistov, I., Liu, J., Harris, J.L., and Young, P.P. (2016). Temporary, Systemic Inhibition of the WNT/β-Catenin Pathway promotes Regenerative Cardiac Repair following Myocardial Infarct. Cell Stem Cells Regen. Med. *2*.
16. Daskalopoulos, E.P., Hermans, K.C., Janssen, B.J., and Matthijs Blankesteijn, W. (2013). Targeting the Wnt/frizzled signaling pathway after myocardial infarction: a new tool in the therapeutic toolbox? Trends Cardiovasc. Med. *23*, 121–127.
17. Coscio, A., Chang, D.W., Roth, J.A., Ye, Y., Gu, J., Yang, P., and Wu, X. (2014). Genetic variants of the Wnt signaling pathway as predictors of recurrence and survival in early-stage non-small cell lung cancer patients. Carcinogenesis *35*, 1284–1291.
18. Song, L., Liu, D., Wang, B., He, J., Zhang, S., Dai, Z., Ma, X., and Wang, X. (2015). miR-494 suppresses the progression of breast cancer in vitro by targeting CXCR4 through the Wnt/β-catenin signaling pathway. Oncol. Rep. *34*, 525–531.
19. Zhou, Y., Zhang, X., Zhang, J., Fang, J., Ge, Z., and Li, X. (2017). LRG1 promotes proliferation and inhibits apoptosis in colorectal cancer cells via RUNX1 activation. PLoS ONE *12*, e0175122.
20. ur Rahman, H., Khan, S.B., Noor, L., Hadi, A., Nawaz, T., Shah, S.T., Abbas, F., and Hafizullah, M. (2011). Assessment of left ventricular systolic and diastolic function by tissue Doppler imaging after acute myocardial infarction. J. Ayub Med. Coll. Abbottabad *23*, 108–111.
21. Verma, A., Meris, A., Skali, H., Ghali, J.K., Arnold, J.M., Bourgoun, M., Velazquez, E.J., McMurray, J.J., Kober, L., Pfeffer, M.A., et al. (2008). Prognostic implications of left ventricular mass and geometry following myocardial infarction: the VALIANT (VALsartan In Acute myocardial iNfarcTion) Echocardiographic Study. JACC Cardiovasc. Imaging *1*, 582–591.
22. Luo, K.Q., Long, H.B., and Xu, B.C. (2015). Reduced apoptosis after acute myocardial infarction by simvastatin. Cell Biochem. Biophys. *71*, 735–740.
23. Han, A., Lu, Y., Zheng, Q., Zhang, J., Zhao, Y., Zhao, M., and Cui, X. (2018). Qiliqiangxin Attenuates Cardiac Remodeling via Inhibition of TGF-β1/Smad3 and NF-κB Signaling Pathways in a Rat Model of Myocardial Infarction. Cell. Physiol. Biochem. *45*, 1797–1806.
24. de Lima, A.D., Guido, M.C., Tavares, E.R., Carvalho, P.O., Marques, A.F., de Melo, M.D.T., Salemi, V.M.C., Kalil-Filho, R., and Maranhão, R.C. (2018). The Expression of Lipoprotein Receptors Is Increased in the Infarcted Area After Myocardial Infarction Induced in Rats With Cardiac Dysfunction. Lipids *53*, 177–187.
25. Diakos, C., Zhong, S., Xiao, Y., Zhou, M., Vasconcelos, G.M., Krapf, G., Yeh, R.F., Zheng, S., Kang, M., Wiencke, J.K., et al. (2010). TEL-AML1 regulation of survivin and apoptosis via miRNA-494 and miRNA-320a. Blood *116*, 4885–4893.
26. Matsudaira, K., Maeda, K., Okumura, N., Yoshikawa, D., Morita, Y., Mitsuhashi, H., Ishii, H., Kondo, T., and Murohara, T.; Nagoya Acute Myocardial Infarction Study (NAMIS) Group (2012). Impact of low levels of vascular endothelial growth factor after myocardial infarction on 6-month clinical outcome. Results from the Nagoya Acute Myocardial Infarction Study. Circ. J. *76*, 1509–1516.
27. Yamamoto, M., Takahashi, T., Serada, S., Sugase, T., Tanaka, K., Miyazaki, Y., Makino, T., Kurokawa, Y., Yamasaki, M., Nakajima, K., et al. (2017). Overexpression of leucine-rich α2-glycoprotein-1 is a prognostic marker and enhances tumor migration in gastric cancer. Cancer Sci. *108*, 2052–2060.
28. Zhao, Q.-F., Du, J., Wu, G.-W., and Hu, X.-D. (2011). Wnt-1 and β-catenin mRNA expressions in rats' myocardial tissue after acute myocardial infarction. Chin. J. Emerg. Med. *20*, 489–493.
29. Virag, J.A., Rolle, M.L., Reece, J., Hardouin, S., Feigl, E.O., and Murry, C.E. (2007). Fibroblast growth factor-2 regulates myocardial infarct repair: effects on cell proliferation, scar contraction, and ventricular function. Am. J. Pathol. *171*, 1431–1440.
30. Peng, L., Ye, L., Dong, G., Ren, L.B., Wang, C.L., Xu, P., and Zhou, X.D. (2009). WNT5A inhibits human dental papilla cell proliferation and migration. Biochem. Biophys. Res. Commun. *390*, 1072–1078.
31. Zhao, X., Zhou, Y., Chen, Y.U., and Yu, F. (2016). miR-494 inhibits ovarian cancer cell proliferation and promotes apoptosis by targeting FGFR2. Oncol. Lett. *11*, 4245–4251.
32. Liu, Y., Li, X., Zhu, S., Zhang, J.G., Yang, M., Qin, Q., Deng, S.C., Wang, B., Tian, K., Liu, L., et al. (2015). Ectopic expression of miR-494 inhibited the proliferation, invasion and chemoresistance of pancreatic cancer by regulating SIRT1 and c-Myc. Gene Ther. *22*, 729–738.
33. Liu, K., Liu, S., Zhang, W., Jia, B., Tan, L., Jin, Z., and Liu, Y. (2015). miR-494 promotes cell proliferation, migration and invasion, and increased sorafenib resistance in hepatocellular carcinoma by targeting PTEN. Oncol. Rep. *34*, 1003–1010.
34. Wang, Y., Xu, J., Zhang, X., Wang, C., Huang, Y., Dai, K., and Zhang, X. (2017). TNF-α-induced LRG1 promotes angiogenesis and mesenchymal stem cell migration in the subchondral bone during osteoarthritis. Cell Death Dis. *8*, e2715.

35. Hao, L., Xie, H., Zhang, B., Chen, D., Wang, S., Zhang, H., and He, S. (2016). LRG1 downregulation in allergic airway disorders and its expression in peripheral blood and tissue cells. J. Transl. Med. *14*, 202.

36. Zhang, Y., Luo, Q., Wang, N., Hu, F., Jin, H., Ge, T., Wang, C., and Qin, W. (2015). LRG1 suppresses the migration and invasion of hepatocellular carcinoma cells. Med. Oncol. *32*, 146.

37. Fujita, A., Sato, J.R., Rodrigues, Lde.O., Ferreira, C.E., and Sogayar, M.C. (2006). Evaluating different methods of microarray data normalization. BMC Bioinformatics *7*, 469.

38. Smyth, G.K. (2004). Linear models and empirical bayes methods for assessing differential expression in microarray experiments. Stat Appl Genet Mol Biol *3*, Article3.

OMTN, Volume *18*

Supplemental Information

MicroRNA-494 Inhibits the LRG1 Expression to Induce Proliferation and Migration of VECs in Rats following Myocardial Infarction

Qiang Su, Xiang-Wei Lv, Yu-Han Sun, Zi-Liang Ye, Bing-Hui Kong, and Zhen-Bai Qin

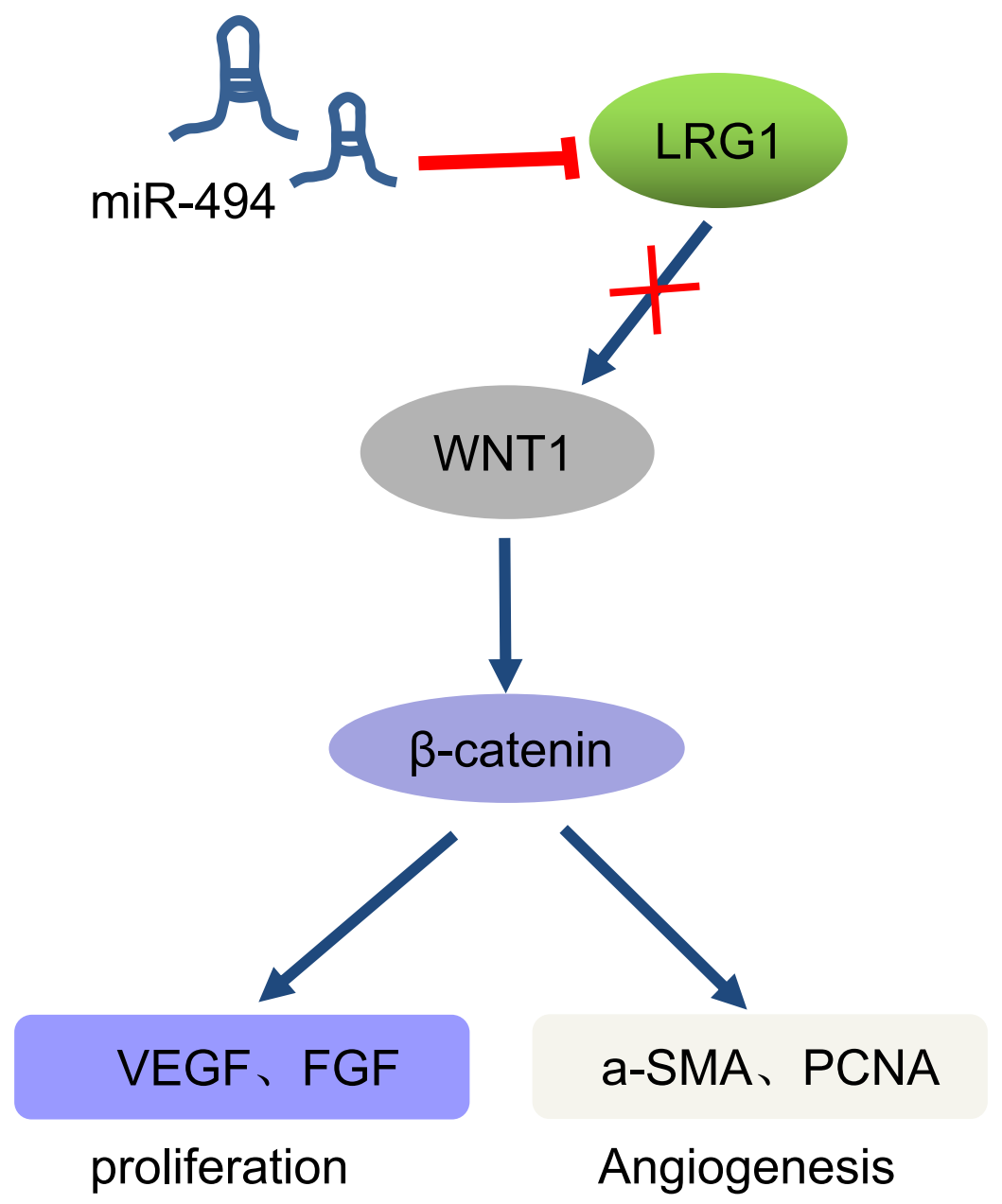
miR-494
LRG1
WNT1
β-catenin
VEGF、FGF
a-SMA、PCNA
proliferation
Angiogenesis